Article

Upconversion Nanoparticles as Imaging Agents for Dental Caries

Julia C. Bulmahn, Andrey N. Kuzmin, Carol Parker, Robert J. Genco, Hilliard L. Kutscher, and Paras N. Prasad*

Read Online

ACCESS | Metrics & More | Article Recommendations

ABSTRACT: Dental caries (cavities) is the most prevalent disease worldwide; however, current detection methods suffer from issues associated with sensitivity, subjective interpretations, and false positive identification of carious lesions. Therefore, there is a great need for the development of more sensitive, noninvasive imaging methods. The 30 nm core@shell $NaYF_4$; Yb20%, Er2%@$NaYF_4$ upconversion nanoparticles (UCNPs), exhibiting strong upconversion emission from erbium upon excitation at 975 nm, were used in the imaging of locations of demineralized enamel and oral biofilm formation for the detection of dental caries. UCNPs were modified with poly(acrylic acid) (PAA) or poly-D-lysine (PDL), and targeting peptides were conjugated to their surface with affinity for either hydroxyapatite (HA), the material dentin is composed of, or the caries causing bacteria *Streptococcus mutans*. A statistical difference in the binding of targeted vs nontargeted UCNPs to HA was observed after 15 min, using both upconversion fluorescence of UCNP ($p < 0.001$) and elemental analysis ($p = 0.0091$). Additionally, using the HA targeted UCNPs, holes drilled in the enamel of bovine teeth with diameters of 1.0 and 0.5 mm were visible by the green emission after a 20 min incubation with no observable nonspecific binding. A statistical difference was also observed in the binding of targeted versus nontargeted UCNPs to *S. mutans* biofilms. This difference was observed after 15 min, using the fluorescence measurements ($p = 0.0125$), and only 10 min ($p < 0.001$) using elemental analysis via ICP-OES measurements of Y^{3+} concentration present in the biofilms. These results highlight the potential of these UCNPs for use in noninvasive imaging diagnosis of oral disease.

KEYWORDS: *upconversion, nanoparticles, imaging, dental caries, peptide targeting*

Noninvasive, early dental caries detection

975 nm → 540 nm
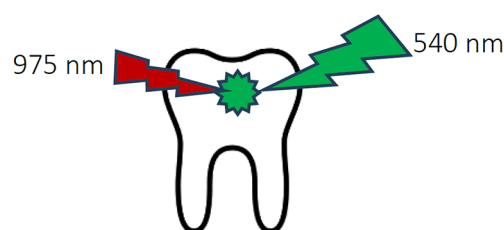
INTRODUCTION

As the most prevalent chronic disease worldwide, dental caries is a substantial burden to both public health and the economy. Globally, 2.4 billion people of all ages are affected by untreated caries in permanent teeth, while 621 million children are affected by untreated caries in primary teeth.[1] Although data on costs specifically related to dental caries are limited, dental diseases cost the world $442 billion in 2010.[2] According to the Centers for Disease Control and Prevention, over 34 million school hours and over $45 billion in productivity are lost in the United States each year due to unplanned or emergency dental care and untreated oral diseases.[3] To address this issue, it is important to develop a capability to detect slow growing noncavitated lesions and to enable nonoperative preventive strategies to suppress their growth.

Currently, dental caries are detected by visual inspection with subjective assessments of color, translucency, and dental hardness, as well as with radiographic images.[4] But even radiographic methods cannot confidently identify cavitation, and most proximal surfaces are not clinically accessible for visual inspection.[4−6] Traditional optical techniques of detection using fluorescence in the visible range of emission demonstrate high sensitivity and specificity, but can result in false positives due to tissue absorption and light scattering.[7] Also, common techniques used by dental practitioners are highly dependent on subjective interpretation, and discrepancies among dentists' diagnoses tend to be frequent.

Nanotechnology is expected to make a major impact on dentistry, with applications including preventive care, dental restoration, delivery of local anesthesia and/or antibiotics, and treatment of various dental diseases.[8] Lanthanide doped upconversion nanoparticles (UCNPs) show promise for these applications due to their uniquely customizable emission spectra, which can be controlled by modification of structure and dopant content, allowing the photoluminescence (PL) to be tuned from deep UV to the short wave infrared (IR) region.
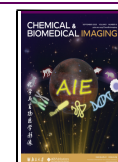
Additionally, these UCNPs absorb near-infrared (NIR, 700–1100 nm) light in the first biological optical transparency window from 650 to 1000 nm, which exhibits deep light penetration. This leads to an increase in the dental tissue penetration depth and an improved signal-to-noise ratio as a result of minimal tissue autofluorescence and reduced scatter.[9] This unique feature allows these UCNPs to be used as superior probes for high contrast optical bioimaging. Through a wide range of surface functionalization techniques, these UCNPs can be effectively coupled to various ligands, enabling site specific labeling of disease causing microbes.[10]

Herein we demonstrate the detection of areas of demineralized enamel and caries causing biofilms using visible green emission from core@shell NaYF$_4$; Yb20%, Er2%@ NaYF$_4$ UCNPs targeted to either the surface of *Streptococcus mutans*, a common bacterium that is a strong acid producer and, along with *Lactobacilli*, considered to play a significant role in the formation of dental caries;[11] or targeted to hydroxyapatite, the mineral dentin is composed of, indicating enamel loss.[12] This suggests their potential for use in the detection of dental caries or other oral diseases. Therefore, these biocompatible UCNPs provide unique noninvasive diagnostic opportunities for modern dentistry.

■ MATERIALS AND METHODS

Materials

Yttrium(III) chloride hexahydrate (YCl$_3$·6H$_2$O, 99.99%), ytterbium(III) chloride hexahydrate (YbCl$_3$·6H$_2$O, 99.9%), erbium(III) chloride hexahydrate (ErCl$_3$·6H$_2$O, 99.9%), ytterbium(III) oxide (Yb$_2$O$_3$, 99.9%), ammonium fluoride (99.99), sodium hydroxide (97%), trifluoroacetic acid (CF$_3$COOH, 99%), sodium trifluoroacetate (CF$_3$COONa, 98%), oleic acid (OA, 90% tech grade), 1-octadecene (ODE, 90% tech grade), poly(acrylic acid) (PAA), 1-ethyl-3-(3-(dimethylamino)propyl)carbodiimide (EDC), N-hydroxysuccinimide (NHS), and sulfosuccinimidyl-4-(N-maleimidomethyl)-cyclohexane-1-carboxylate (sulfo-SMCC) were purchased from MilliporeSigma (St. Louis, MO). Poly-D-lysine (PDL, 30–70 kDa MW), hexane (ACS reagent grade, ≥98.5%), and brain heart infusion (BHI) broth were purchased from Fisher Scientific (Waltham, MA). Gadolinium (Gd^{3+}), yttrium (Y^{3+}), and ytterbium (Yb^{3+}) standards for ICP were purchased from Inorganic Ventures (Christiansburg, VA). High purity nitric acid (HNO$_3$, BDH Aristar Plus) for quantitative trace metal analysis was purchased from VWR (Radnor, PA). Ethanol (anhydrous, 200 proof) was purchased from Decon Laboratories (King of Prussia, PA). Hydroxyapatite (HA) discs (9.5 mm diameter × 1.8 mm thick) were purchased from Himed (Old Bethpage, NY). Peptides (Pep1 sequence: DDSWDTNDANVVC-RQLGA; and Pep2 sequence: QGRVEVLYRGSWGTVC) were purchased from GenScript (Piscataway, NJ). *S. mutans* was purchased from ATCC (Manassas VA). All materials were used as received.

Methods

A core@shell UCNP architecture was used to optimize the optical properties of the UCNPs for maximum green fluorescence upconversion efficiency. To avoid nonradiative surface quenching effects caused by large defects in the outer surface of the nanoparticle, the sensitizer (Yb^{3+}) and activator (Er^{3+}) ions were doped into the core structure, which was then coated with an inert NaYF$_4$ shell.[13] Core@shell NaYF$_4$; Yb20%, Er2%@NaYF$_4$ UCNPs were synthesized through a combination of coprecipitation and thermal decomposition methods[14,15] as described below.

Synthesis of NaYF$_4$; Yb20%, Er2% Core. Core UCNPs were synthesized through room temperature coprecipitation, followed by Ostwald ripening. YCl$_3$·6H$_2$O (0.78 mmol), YbCl$_3$·6H$_2$O (0.20 mmol), and ErCl$_3$·6H$_2$O (0.02 mmol) were added to a three-neck 100 mL round-bottom flask (RBF) along with 9 mL of OA and 15 mL of ODE. The mixture was heated to 160 °C and held for 1 h under Ar protection, and at constant stirring at 280 rpm to dissolve the lanthanide salts. The mixture was then cooled to room temperature (RT), ~25 °C, followed by the addition of 10 mL of methanol, containing NH$_4$F (4 mmol) and NaOH (2.5 mmol). After addition of the methanol solution, the resulting dispersion was held at RT with constant stirring at 500 rpm for 30 min. This suspension was then heated to 100 °C and held 30 min with constant stirring at 280 rpm to evaporate all methanol. The temperature was subsequently increased to 300 °C and maintained for 1 h under Ar protection. The final suspension was cooled to RT and the resulting UCNPs were precipitated by adding excess ethanol. The precipitate was collected by centrifugation at 7.5K RCF for 5 min and washed twice with ethanol. The resulting OA capped UCNPs were finally dispersed in 10 mL of hexane for further use.

Coating of the Core with a NaYF$_4$ Shell. Growth of the shell was accomplished through the thermolysis of shell precursors, followed by gradual deposition of the shell material onto the previously synthesized core particles. The shell precursor was prepared by mixing Y$_2$O$_3$ (0.25 mmol) with 10 mL of 50% trifluoroacetic acid in a 100 mL three-neck RBF, followed by refluxing at 95 °C until a clear suspension was obtained. Y(CF$_3$COO)$_3$ (0.25 mmol) precursors were obtained by evaporation to dryness using Ar. CF$_3$COONa (1.0 mmol) and 5 mL of the previously prepared core in hexane were then added to the RBF along with 10 mL of OA and 10 mL of ODE. The mixture was then degassed at 120 °C for 30 min under Ar protection with stirring at 280 rpm. The resulting suspension was then heated to 320 °C and kept at this temperature for 30 min before cooling to RT. The resulting OA capped UCNPs were collected by adding an excess amount of ethanol and then centrifuged at 7.5K RCF for 5 min. The collected precipitate was washed twice with ethanol and finally dispersed in 10 mL of hexane for further use.

Ligand Stripping. To prepare UCNPs for ligand stripping, needed to replace the surface with a water compatible polymer, a 10 mg/mL nanoparticle dispersion was prepared in hexane. Stripping of the native oleate ligands was performed through a modified biphasic ligand stripping method, based on a procedure developed by Bogdan et al.,[16] via ligand protonation using 0.1 M hydrochloric acid (HCl). 3.5 mL of UCNPs (10 mg/mL) in hexane, and 3.5 mL of 0.1 M HCl were combined in a glass vial and allowed to stir overnight at 650 rpm. After overnight stirring, the top hexane layer was removed, and the bottom layer was extracted 3 times with diethyl ether to remove the dissociated OA ligands. The UCNPs were collected via centrifugation of the resulting aqueous dispersion at 18K RCF for 15 min. The supernatant was discarded, and the resulting pellet was suspended in 1 mL DI water via sonication. The final suspension of ligand-free water-dispersible UCNPs (~30 mg/mL) was kept at RT for further modification.

Poly-D-lysine Coating. One mL of ligand free UCNPs (~30 mg/mL) and 1 mL of poly-D-lysine (PDL, 2.5 mg/mL) were added to a 20 mL glass vial and allowed to gently stir overnight. The UCNP-NH$_2$ sample was collected via centrifugation at 18K RCF for 15 min. The supernatant was discarded, and the resulting pellet was resuspended in 1 mL of DI water. The resulting suspension was centrifuged at 18K RCF for 15 min. The supernatant was discarded, and the resulting pellet was resuspended in 2 mL of PBS for immediate use.

Peptide Conjugation to UCNP-NH$_2$ Using Sulfo-SMCC. The UCNP-NH$_2$ dispersion (15 mg/mL, 2 mL of PBS) was incubated with 250 µL of 10 mM sulfo-SMCC for 30 min at RT with gentle shaking. Unreacted species were removed by centrifugation twice at 18K RCF for 15 min each time. The collected sulfo-SMCC-activated UCNPs were resuspended in 2 mL of PBS and covalently linked to peptide by adding 500 µL of the peptide suspension (1 mg/mL) and gently stirred for 2 h at RT. The resulting peptide conjugated UCNP (e.g., UCNP-PDL-Pep1) dispersion was washed twice by centrifugation (15 min, 18K RCF), resuspended in Ringer's solution for microbiology, and stored at 4 °C until use.

Polyacrylic Acid Coating. One mL of ligand free UCNPs (~30 mg/mL), 1 mL of poly(acrylic acid) (PAA, 10 mg/mL), and 250 µL of 0.5 M NaOH were added to a glass vial and allowed to gently stir
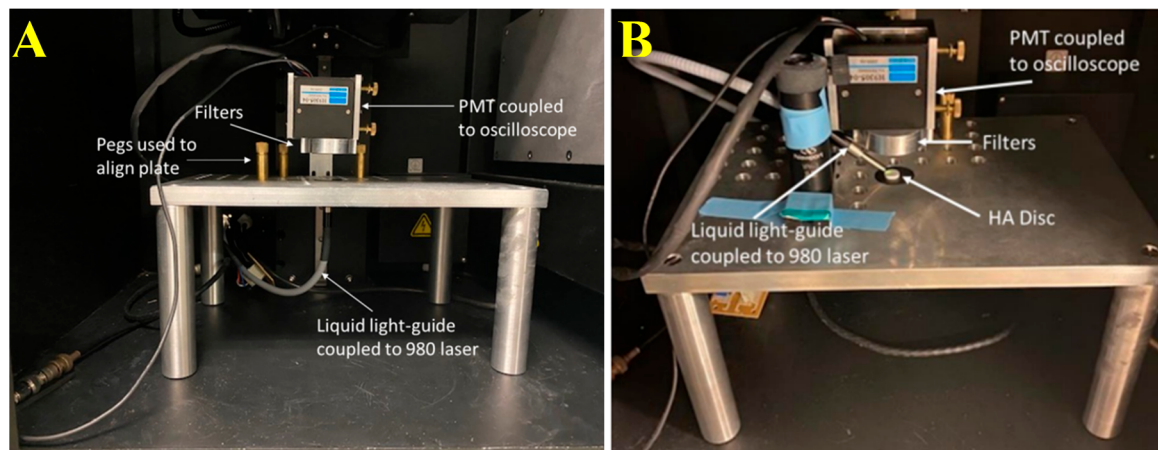
Figure 1. Setup used to evaluate fluorescence intensity (A) in 24-well plates and (B) on HA discs.

overnight. UCNP-COOH were collected via centrifugation at 18K RCF for 15 min. The supernatant was discarded, and the resulting pellet was resuspended in 1 mL of DI water. The resulting suspension was centrifuged at 18K RCF for 15 min. The supernatant was discarded, and the resulting pellet was resuspended in 1 mL of 0.1 M MES buffer pH 5.5 for further use.

Peptide Conjugation to UCNP-COOH Using EDC/NHS. The UCNP-COOH suspension (30 mg/mL, 1 mL of 0.1 M MES pH5.5 buffer) was incubated with 500 μL of 15 mM 1-ethyl-3-(3-(dimethylamino)propyl) carbodiimide hydrochloride (EDC) and 500 μL of 40 mM N-hydroxysuccinimide (NHS) for 15 min at RT with gentle shaking. Unreacted species were removed by centrifugation twice at 18K RCF for 15 min each time. The collected NHS-activated UCNPs were resuspended in 2 mL of PBS and covalently linked to peptide by adding 500 μL of the peptide suspension (1 mg/mL) and gently stirred for 2 h at RT. The resulting peptide conjugated UCNP (e.g., UCNP-PAA-Pep2) dispersion were washed twice by centrifugation (15 min, 18K RCF), resuspended in Ringer's solution for microbiology, and stored at 4 °C until use.

Characterization. The size and morphology of the resulting UCNPs were characterized by transmission electron microscopy (TEM) using a JEM-2010 microscope (JEOL USA, Inc., Peabody, MA) at an acceleration voltage of 200 kV. To prepare UCNPs for TEM, 10 μL of a nanoparticle suspension was dropped onto the surface of a 200-mesh fomvar coated copper grid (Ted Pella Inc., Redding, CA) and the solvent was evaporated at RT before visualization. Hydrodynamic diameter and surface charge of the resulting UCNPs were determined using dynamic light scattering (DLS) and zeta potential analysis performed on a 90Plus zeta sizer (Brookhaven Instruments, Holtsville NY). To prepare samples for testing, 50 μL of the nanoparticle dispersion was added to 2.5 mL of DI water. Photoluminescence (PL) spectra were measured using a FluoroLog-3.1.1 spectrofluorometer (Horiba Scientific, Jobin Yvon, Edison, NJ), with a slit width defining a spectral resolution of 5 nm. The excitation source was a 975 nm fiber-coupled laser diode (BWT Beijing Ltd., Beijing, China). Elemental analysis was performed using a Thermo Scientific iCAP 6000 Inductively Coupled Plasma Optical Emission Spectrometer (ICP-OES). Samples were digested overnight in 500 μL of HNO$_3$ and diluted to a final volume of 15 mL with 2% HNO$_3$. Elemental standards were prepared by using the same 2% HNO$_3$ solution.

Determining Concentration and Power Settings for Imaging. A 300 μL UCNP suspension containing 125, 250, 500, or 1000 μg/mL Y^{3+} was added to the wells of a 96 well plate, and the luminescence emission intensity was recorded at power densities of 1.30, 1.95, 2.60, 3.25, and 3.90 W/cm^2, using an imaging system consisting of a 975 nm laser diode coupled to a liquid light guide (Thor Laboratories, Newton, NJ), and a PMT (H9305−04, Hamamatsu, Japan) equipped with an 842 nm short pass filter (Semrock, Rochester, NY) to ensure filtration of the excitation light to

record emission. The PMT was coupled to an oscilloscope (TDS 2012, Tektronix, Beaverton, OR) that was used to quantify the fluorescence intensity (Figure 1). Additionally, the plate was dried in a 60 °C oven for 3 h to evaporate the excess water and imaged again. Based on the data obtained, experiments were performed using a nanoparticle concentration equivalent to 1000 μg/mL Y^{3+}.

Evaluating the Binding Efficiency of UCNP-PDL-Pep1 to Hydroxyapatite Using Fluorescence. HA discs (9.5 mm diameter × 1.8 mm thick) were incubated with 300 μL of targeted and nontargeted UCNPs, at a concentration of 1 mg/mL Y^{3+}, for 5, 10, 15, 30, 45, and 60 min. At each time point, the NP suspension was removed and the HA discs were washed twice with 500 μL of Ringer's for microbiology. The HA discs were then imaged using a power density of 3.0 W/cm^2 and an imaging system set up very similar to that used for previous fluorescence measurements however the excitation source was positioned above the HA disc rather than below (Figure 1B).

Evaluating the Binding Efficiency of UCNP-PDL-Pep1 to Hydroxyapatite Using Y^{3+} Concentration. After evaluating the fluorescent intensity present on the HA discs surface upon excitation at 975 nm, they were added to 15 mL centrifuge tubes containing 500 μL of concentrated HNO$_3$ with a known amount of Gd^{3+} (used as the internal standard) and incubated for 1 h. The HA discs were then removed, and the resulting suspension was diluted to a final volume of 15 mL of 2% HNO$_3$. The concentration of Y^{3+} was evaluated using ICP-OES and the % bound was determined based on the amount of Y^{3+} present in the original UCNP suspension.

Binding of UCNP-PDL-Pep1 to Bovine Teeth. Bovine teeth were locally sourced, and 1.0 and 0.5 mm holes were drilled in the enamel, exposing the dentin of the teeth. The teeth were incubated for 20 min with UCNP-PDL-Pep1 (300 μL). After the incubation period, the teeth were rinsed in 5 mL of Ringer's for microbiology for 5 min on a rocker to remove unbound UCNPs. To obtain an image of each tooth, a Maestro small animal imaging system (Cambridge Research and Instrumentation, Boston, MA) equipped with a 503−555 nm band-pass filter to isolate the 540 nm green emission from Er, and a 975 nm laser diode coupled to a liquid light guide to generate this upconverted green fluorescence, was used.

Growth Conditions of *S. mutans* Biofilms. To evaluate the binding of UCNP-PAA-Pep2 to *S. mutans*, biofilms were grown in 24 well tissue culture plates (Costar, Corning Life Sciences, Corning, NY) *S. mutans* was prepared by suspending a few colonies previously grown on brain heart infusion (BHI) agar plates in 10 mL of BHI broth. This suspension was incubated for 6 h at 37 °C and 5% CO$_2$. After incubation, the OD at 600 nm was adjusted to 0.5, and the resulting suspension was diluted 1:100 in BHI broth. To prepare the plates for biofilm growth, wells were precoated with saliva. Saliva was collected, centrifuged for 30 min @ 27000 × g and 0.22 μm filtered, and 0.5 mL was added to each well. After incubating for 4 h at RT with gentle shaking, the saliva was removed and replaced with 500 μL
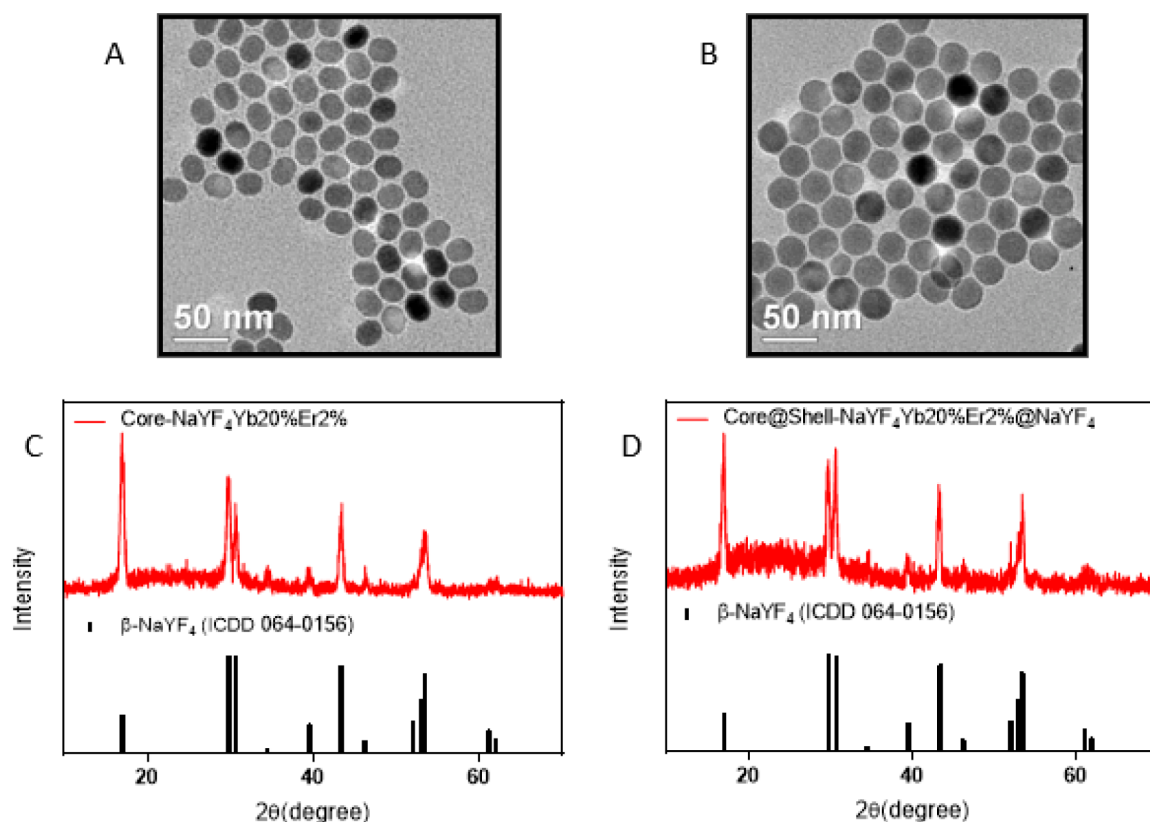
Figure 2. TEM images and XRD patterns of core $NaYF_4$; Yb20%, Er2% (A, C); and core@shell $NaYF_4$; Yb20%, Er2%@$NaYF_4$ (B and D).

of BHI broth and 500 μL of saliva. 500 μL of the previously prepared *S. mutans* culture was added, and the plates were then incubated for 48 h at 37 °C and 5% CO_2. Media was removed and fresh 500 μL BHI broth and 500 μL saliva was added daily. 48-h biofilms were used for all experiments.

Evaluating the Binding Efficiency of UCNP-PAA-Pep2 to *S. mutans* Using Fluorescence. *S. mutans* biofilms grown in 24- well plates were incubated with 300 μL of targeted and nontargeted UCNPs, at a concentration of 1 mg/mL Y^{3+}, for 5, 10, 15, 30, 45, and 60 min. At each time point, the NP suspension was removed, and the wells were washed twice with 500 μL of Ringer's for microbiology. The plate was dried overnight, and the wells were then imaged at a power density of 3.0 W/cm^2 using the same imaging system used to quantify the Er green fluorescence intensity as a ratio of Y^{3+} concentration (Figure 1).

Evaluating the Binding Efficiency of UCNP-PAA-Pep2 to *S. mutans* Using the Y^{3+} Concentration. After the fluorescent intensity present on the biofilm surface upon excitation at 975 nm was evaluated, 500 μL of concentrated HNO_3 with a known amount of Gd^{3+} (used as the internal standard) was added to each well and incubated for 1 h. The sample suspensions were collected and transferred to a 15 mL centrifuge tubes. The wells were washed with 500 μL Ringer's for microbiology which was also added to its respective sample tube. The resulting suspensions were diluted to a final volume of 15 mL with 2% HNO_3. The concentration of Y^{3+} was evaluated using ICP-OES and the % bound was determined based on the amount of Y^{3+} present in the original NP suspension.

■ RESULTS

Characterization of Upconversion Nanoparticles

As synthesized core particles were determined via TEM to be 24 $\pm$ 1 nm (Figure 2A). Formation of the β-phase was confirmed by powder XRD (Figure 2C). The as synthesized $NaYF_4$; Yb20%, Er2%@$NaYF_4$ core@shell UCNPs were determined via TEM to be 31 $\pm$ 2 nm (Figure 2B), and

formation of β-phase core@shell particles was confirmed by XRD (Figure 2D).

The optical properties of these UCNPs are a result of energy transfer upconversion (ETU) and excited state absorption (ESA) processes involving Yb^{3+} and Er^{3+}. The emission peaks at 420, 540, and 660 nm are a result of the $^2H_{9/2} \rightarrow {}^4I_{15/2}$, $^2H_{11/2}$, $^4S_{3/2} \rightarrow {}^4I_{15/2}$, and $^4F_{9/2} \rightarrow {}^4I_{15/2}$ transitions of Er^{3+}, respectively.[17,18] Due to the 20:2 ratio of Yb^{3+} to Er^{3+}, the emission of these UCNPs appears visibly green. Changing this ratio alters the energy transfer efficiency from Yb^{3+} to Er^{3+}, and visible emissions ranging from green to red light can be obtained.[17] For imaging, we chose to use 540 nm (green) emission as this is the stronger emission peak, and it is easier for the human eye to visualize green light.

UCNP emission intensity increases as a function of size. Ultrasmall <5 nm UCNPs do not exhibit visible luminescence upon 975 nm excitation. UCNPs begin to exhibit luminescence around 10 nm, we have found optimal UCNP luminescence for this project to occur when NPs are approximately 30 nm.[19] This size demonstrates strong visible green emission, and the synthesis method results in reproducible size and morphology. Synthesis of NPs greater than 50 nm in size has proven less reproducible; therefore, 30−35 nm UCNPs were used for this work.

Bioconjugation

To convert the as synthesized oleic acid (OA)-capped particles to a hydrophilic surface for translational biological applications, the surface ligand was removed and replaced with poly(acrylic acid) (PAA) or poly-D-lysine (PDL). A biphasic ligand stripping method, as described in the experimental section, was used to enable water dispersibility of the UCNPs.[16] Briefly, using dilute HCl, the hydrophobic OA surface ligands were
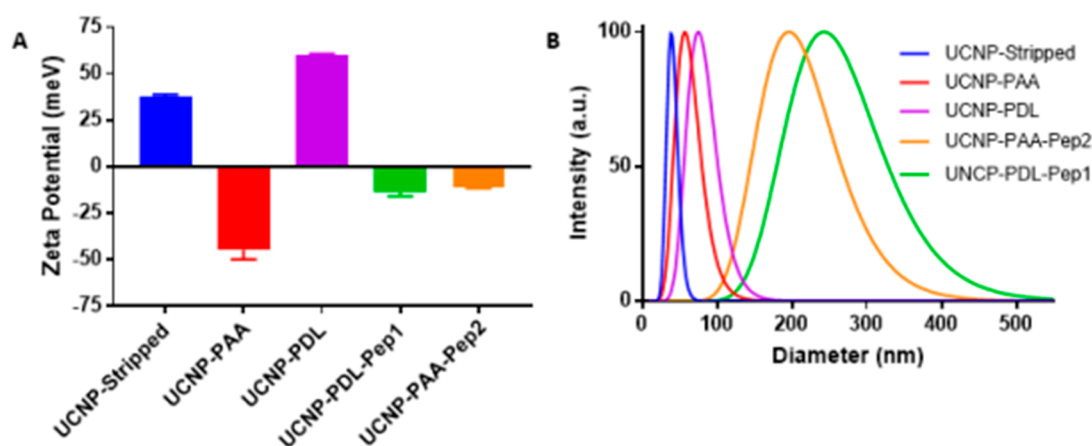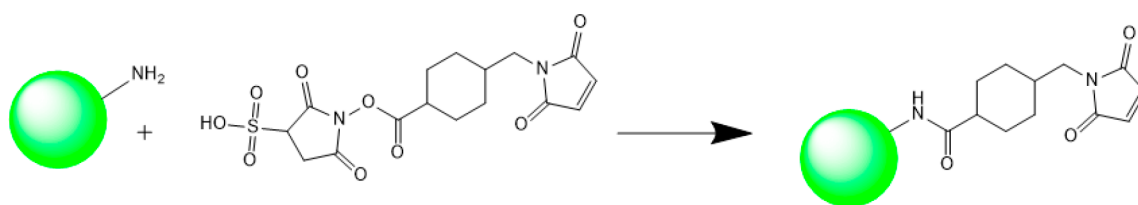
Figure 3. (A) Zeta potential measurement and (B) hydrodynamic diameter, measured by DLS, of UCNP-Stripped (blue), UCNP-PAA (red), UCNP-PDL (purple), UCNP-PDL-Pep1 (green), and UCNP-PAA-Pep2 (orange).

Scheme 1. Schematic of the Reaction between Sulfo-SMCC and UCNP-NH$_2$ to Produce a Maleimide Activated Intermediate

Scheme 2. Schematic of the Reaction between Maleimide Activated UCNP and Pep1
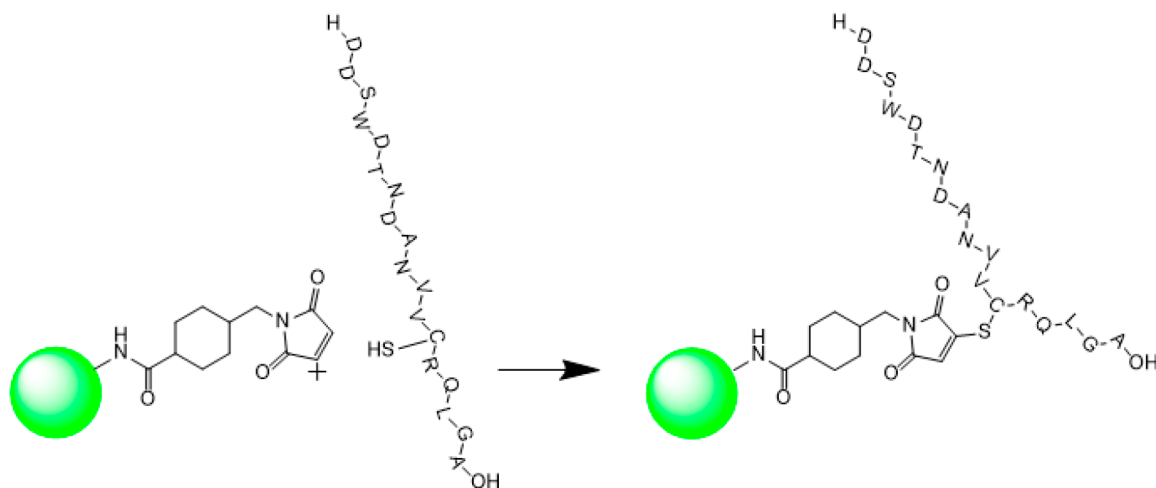

protonated, leading to their dissociation from the nanoparticle surface and the successive transfer of UCNPs from hexane to the aqueous phase.[16] This process results in a highly colloidally stable aqueous dispersion of UCNPs, with a zeta potential of +37.5 ± 1 meV and a mean hydrodynamic diameter of 39 nm (Figure 3), which can then be modified with a new surface coating for the required application, in this case peptide conjugation.

For evaluation of UCNP binding to demineralized enamel, we chose to use a peptide targeting hydroxyapatite, the mineral of which dentin is composed. The peptide used, Pep1, has a peptide sequence of DDSWDTNDANVVCRQLGA, and is a peptide fragment of salivary agglutinin (SAG), a glycoprotein abundant in human saliva, with high affinity to hydroxyapatite. For evaluation of UCNP binding to caries causing biofilms we chose to use a peptide targeting *S. mutans*. The peptide used,

Pep2, has a peptide sequence of QGRVEVLYRGSWGTVC, and is a peptide fragment of SAG with high affinity to *S. mutans*.[12]

PDL was chosen to provide surface available −NH$_2$ functional groups to facilitate peptide conjugation utilizing sulfosuccinimidyl-4-(*N*-maleimidomethyl) cyclohexane-1-carboxylate (sulfo-SMCC) cross-linker chemistry. Successful surface coating of the UCNPs with PDL was confirmed by an increase in zeta potential to +59.6 ± 1 meV, and an increase in mean hydrodynamic diameter to 75 nm (Figure 3). Schemes 1 and 2 demonstrate the maleimide activation of the amine groups on the nanoparticle surface using sulfo-SMCC, and the reactions between Pep1 and maleimide activated UCNP-NH$_2$. Successful attachment of Pep1 to UCNP-PDL was confirmed by a decrease in zeta potential to −13.7 ± 2 meV and an

Scheme 3. Schematic of the Reaction between EDC/Sulfo-NHS and UCNP-COOH to Produce an Sulfo-NHS Ester Intermediate
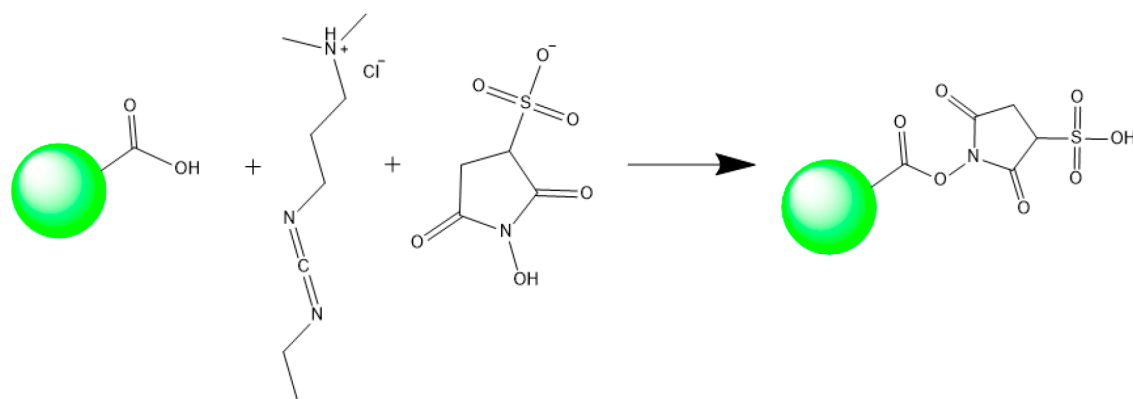
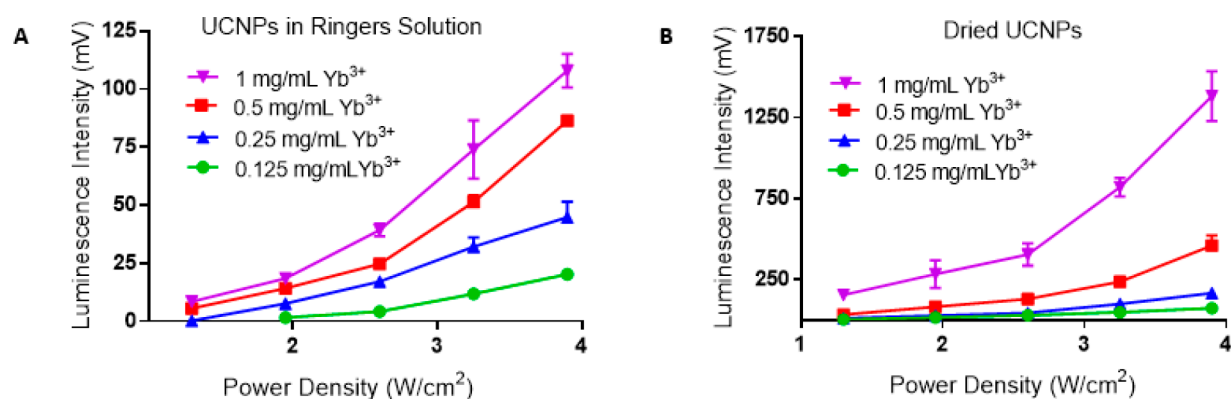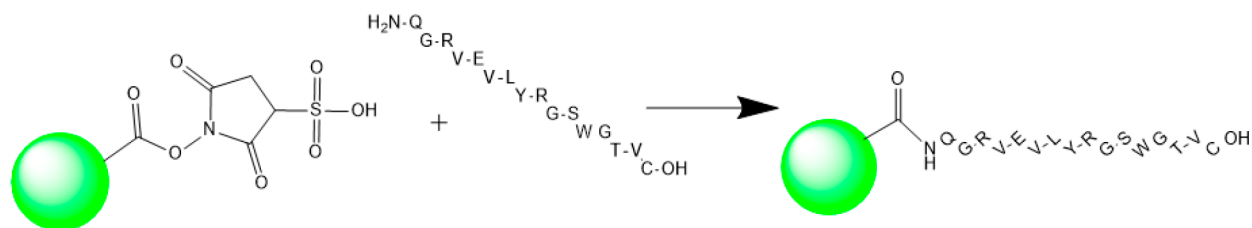**Scheme 4. Schematic of the Reaction between Sulfo-NHS Activated UCNP and Pep2**

Figure 4. Emission intensity of 300 μL of UCNP suspension containing 0.125, 0.25, 0.50, and 1.00 mg/mL Y^{3+} (A) in Ringer's solution for microbiology and (B) dried at 60 °C for 3 h, excited using power densities of 1.30, 1.95, 2.60, 3.25, and 3.90 W/cm^2.

increase in mean hydrodynamic diameter to 241 nm (Figure 3).

PAA was used to provide surface available −COOH functional groups to facilitate peptide conjugation based on a modified method utilizing the well-established 1-ethyl-3-(3-(dimethylamino)propyl) carbodiimide hydrochloride (EDC), *N*-hydroxysuccinimide cross-linking chemistry. Successful surface coating of the UCNPs with PAA was confirmed by a decrease in zeta potential to −44.9 ± 5 meV and an increase in mean hydrodynamic diameter to 56 nm (Figure 3). Schemes 3 and 4 demonstrate the activation of the carboxyl groups on the nanoparticle surface using EDC/NHS, and the reaction between Pep2 and sulfo-NHS activated UCNP-COOH. Successful attachment of Pep2 to UCNP-PAA was confirmed by an increase in zeta potential to −10.9 ± 1 meV and an increase in mean hydrodynamic diameter to 195 nm (Figure 3).

Determining UCNP Concentration and Imaging Settings

We created an imaging system using a 975 nm laser diode coupled to a light guide for excitation and a PMT coupled to an oscilloscope as a detector (Figure 1). To determine minimal and optimal power necessary to generate luminescence, we evaluated the emission intensity of varying concentrations of UCNPs represented as the concentration of Y^{3+} (the most abundant metal in the UCNP formulation) vs the power density of the laser diode. We evaluated concentrations of 0.125, 0.25, 0.50, and 1.0 mg/mL using power densities of 1.30, 1.95, 2.60, 3.25, and 3.90 W/cm^2. A significant difference was observed between the emission of the UCNPs in suspension and the UCNPs dried, which was significantly brighter (Figure 4A and B); therefore, we decided to image the biofilms dry. A 108 mV emission intensity was observed from 1 mg/mL UCNPs in suspension excited at a power density of 3.90 W/cm^2 which is equivalent to that observed from 250 μg/mL dried when excited at 3.25 W/cm^2. Based on the intensity
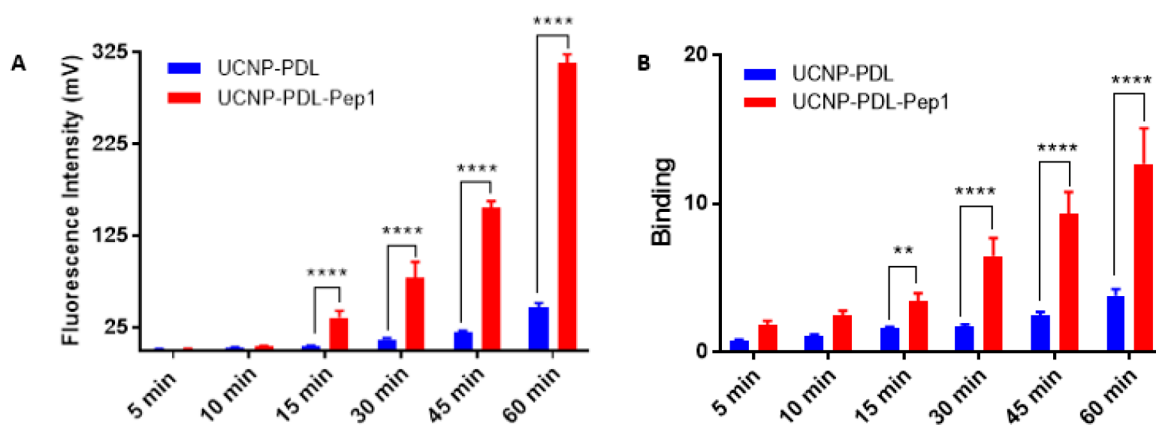
Figure 5. (A) Fluorescence intensity and (B) binding efficiency UCNP-PDL and UCNP-PDL-Pep1 to HA discs at 5, 10, 15, 30, 45, and 60 min (concentration of UCNPs equivalent to 1 mg/mL Y^{3+}).
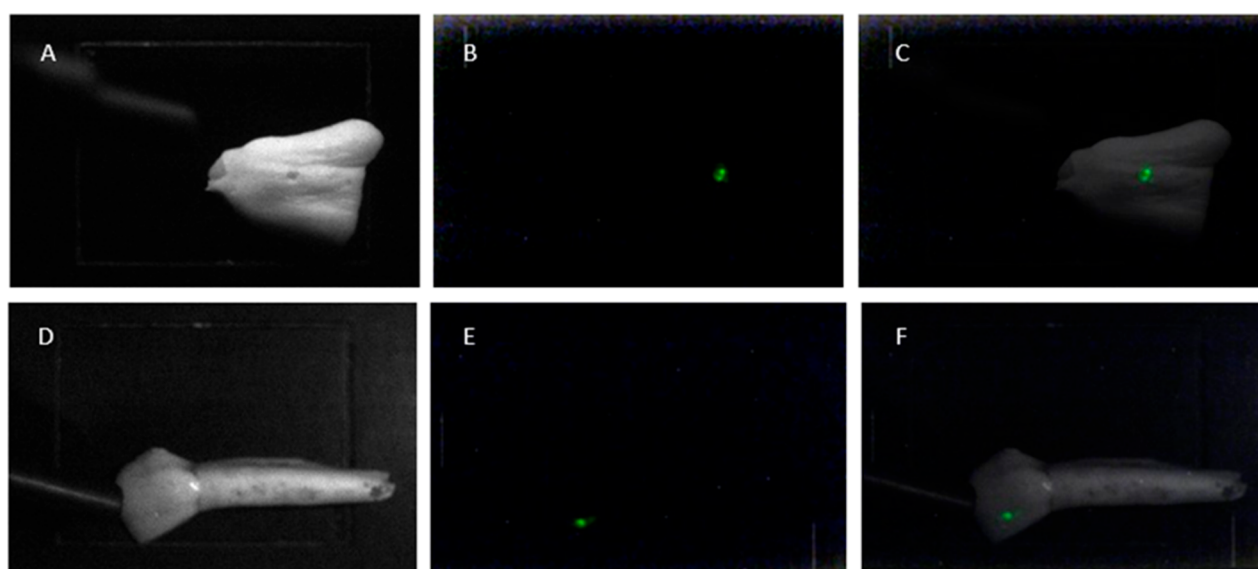

Figure 6. Bright field (right), fluorescence (center), and merged (right) images of a bovine tooth with 1.0 mm (A−C) and 0.5 mm (D−F) holes drilled through the enamel incubated with UCNP-PDL-Pep1 for 20 min at 37 °C.

of observed emission, we chose to use UCNPs at a concentration of 1 mg/mL Y^{3+} and a power density of 3.0 W/cm² to obtain the most observable difference in binding of targeted vs nontargeted UCNPs. This also most closely resembles the conditions under which imaging would occur in the mouth, as the biofilms would not be submerged under 1−2 cm of liquid, rather they would be at the surface of the tooth exposed to air or the oral cavity.

Hydroxyapatite Binding Efficiency of UCNP-PDL-Pep1

To determine the binding efficiency of targeted UCNPs to demineralized enamel, HA discs were incubated with UCNP-PDL-Pep1 and UCNP-PDL, at a concentration of 1 mg/mL Y^{3+}, for 5, 10, 15, 30, 45, and 60 min. After each incubation, the discs were rinsed, and emission intensity and percentage of UCNP bound based on Y^{3+} concentration was evaluated. An observable difference in the green fluorescence intensity of the emission from the HA discs incubated with UCNP-PDL (4.5 mV) and UCNP-PDL-Pep1 (36 mV) was seen after 15 min (Figure 5A, $p < 0.001$, 2-way ANOVA). This was corroborated through the evaluation of the binding efficiency as determined by ICP-OES elemental analysis of HA disc incubated with UCNP-PDL-Pep1 (3.4%) and UCNP-PDL (1.5%) after 15

min (Figure 5B, $p = 0.0091$, 2-way ANOVA). The green emission intensity and % binding of the HA discs incubated with UCNP-PDL-Pep1 continued to increase while minimal nonspecific binding was observed even after 1 h.

Binding Efficiency of UCNP-PDL-Pep1 in "Demineralized" Teeth

To evaluate the ability of UCNPs-PDL-Pep1 to bind to areas of demineralized enamel in a preliminary ex vivo model, we drilled 1.0- and 0.5 mm holes in extracted bovine teeth. After the enamel was compromised, the teeth were incubated for 20 min with UCNPs-PDL-Pep1 followed by rinsing with PBS. Upon excitation with 975 nm light, we were able to successfully image using green fluorescence, both the 1.0- and 0.5 mm holes in the enamel with no apparent nonspecific binding (Figure 6).

S. mutans Binding Efficiency of UCNP-PAA-Pep2

To determine the binding efficiency of targeted UCNPs for caries causing bacteria, *S. mutans* biofilms were incubated with UCNP-PAA-Pep2 and UCNP-PAA, at a concentration of 1 mg/mL Y^{3+}, for 5, 10, 15, 30, 45, and 60 min. After each incubation, the biofilms were rinsed and dried, and the green
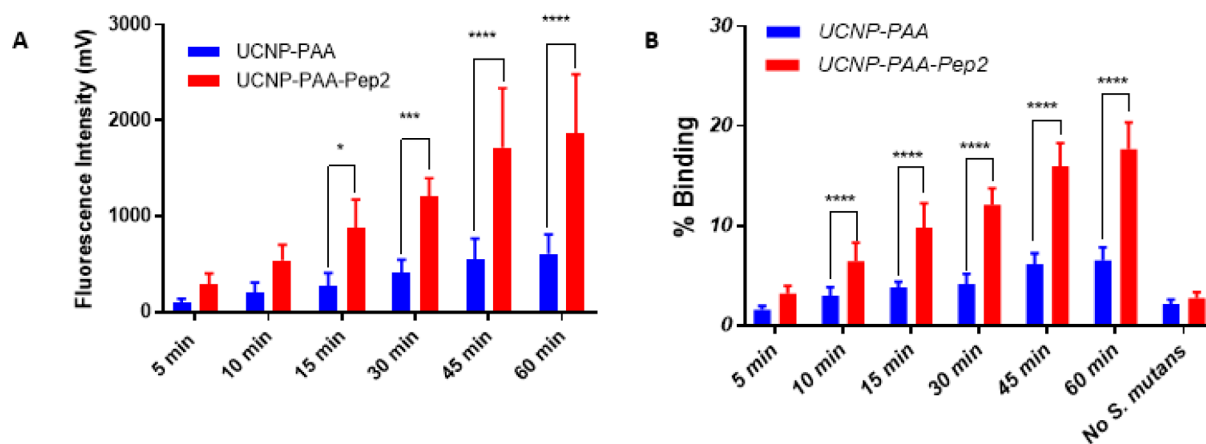
Figure 7. (A) Fluorescence intensity and (B) binding efficiency UCNP-PAA and UCNP-PAA-Pep2 to *S. mutans* biofilms at 5, 10, 15, 30, 45, and 60 min (concentration of UCNPs equivalent to 1 mg/mL Y^{3+}).

emission intensity and percentage of UCNP bound based on the Y^{3+} concentration were evaluated. An observable difference in the fluorescence intensity of the emission from the *S. mutans* biofilms incubated with UCNP-PAA (266 mV) when compared with those incubated with UCNP-PAA-Pep2 (878 mV) was seen after 15 min (Figure 7A, $p = 0.0125$, 2-way ANOVA). This same difference in binding was observable using ICP-OES elemental analysis of the biofilms incubated with UCNP-PAA-Pep2 (6.5%) and UCNP-PAA (3.0%) after 10 min (Figure 7B, $p < 0.001$, 2-way ANOVA). The green emission intensity and percentage of binding of the biofilms incubated with UCNP-PAA-Pep2 continued to increase while minimal nonspecific binding was observed even after 1 h.

DISCUSSION

Despite the fact of strong dependence of UCNP emission intensity on nanoparticle size, we found that the optimum NPs size for dental applications is approximately 30 nm. Smaller sized UCNPs do not demonstrate a strong green emission, while synthesis of NPs greater than 50 nm in size has proven less reproducible.

A statistical difference in the binding of targeted vs nontargeted UCNPs to HA and to *S. mutans* biofilm using both upconversion green fluorescence of UCNPs ($p < 0.001$) and elemental analysis ($p = 0.0091$) using elemental analysis via ICP-OES measurements of Y^{3+} concentration present in the biofilms confirms targeting the UCNPs by Pep1. It demonstrates that effective targeting improves the binding efficiency of UCNPs to HA to discs, simulating demineralized enamel, as well as to areas of demineralized enamel in a preliminary ex vivo model, compared to untargeted UCNPs. This suggests a good potential of the formulation for use in detecting areas of demineralized enamel and early caries to formation of at least 0.5 mm in size.

In the experiments testing the binding efficiency of targeted UCNPs for caries causing bacteria, the use of Pep2 improves the binding efficiency of UCNPs to *S. mutans*, suggesting the potential of this formulation for use in detecting areas of caries causing biofilm growth and, therefore, early caries formation. We initially used the same method to conjugate Pep2 to the surface of the UCNPs as we used for Pep1 however, UCNP-PDL showed significant nonspecific binding to the biofilms in preliminary binding experiments (data not shown). This can be attributed to electrostatic interactions between the biofilm

and UCNP-PDL as the *S. mutans* biofilms exhibit a zeta potential of −15 meV. Therefore, to avoid nonspecific binding, we chose a different EDC/NHS conjugation strategy utilizing PAA coated UCNPs rather than PDL.

CONCLUSION

Unlike conventional fluorescence emission, this upconversion photoluminescence is exhibited at significantly shorter wavelengths than the excitation light.[20] This unique feature allows our UCNPs to be used as superior probes for high contrast optical bioimaging by avoiding issues associated with tissue absorbance and scattering. Using UCNPs conjugated to peptides with affinity to demineralized enamel and caries causing biofilms, we were able to demonstrate the ability of these nanoformulations to successfully bind to HA and *S. mutans* biofilms. Additionally, using HA targeted UCNPs, holes drilled in the enamel of bovine teeth with diameters of 1.0 and 0.5 mm were visible by upconversion green fluorescence after a 20 min incubation with no observable nonspecific binding. Therefore, these biocompatible UCNPs provide unique noninvasive diagnostic opportunities for the imaging and diagnosis of oral diseases and carious lesions.

AUTHOR INFORMATION

Corresponding Author

Paras N. Prasad − *Institute for Lasers, Photonics and Biophotonics, Department of Chemistry, University at Buffalo, The State University of New York, Buffalo, New York 14260, United States; Department of Chemistry, University at Buffalo, The State University of New York, Buffalo, New York 14260, United States;* orcid.org/0000-0002-0905-7084; Email: pnprasad@buffalo.edu

Authors

Julia C. Bulmahn − *Institute for Lasers, Photonics and Biophotonics, Department of Chemistry, University at Buffalo, The State University of New York, Buffalo, New York 14260, United States; Department of Chemistry, University at Buffalo, The State University of New York, Buffalo, New York 14260, United States; Advanced Cytometry Instrumentation System (ACIS), Amherst, New York 14260, United States*

Andrey N. Kuzmin − *Advanced Cytometry Instrumentation System (ACIS), Amherst, New York 14260, United States;* orcid.org/0000-0001-7371-4643

Carol Parker − *Department of Oral Biology, University at Buffalo, The State University of New York, Buffalo, New York 14214, United States*

Robert J. Genco − *Microbiome Center, Department of Oral Biology & Microbiology & Immunology, University at Buffalo, The State University of New York, Buffalo, New York 14214, United States*

Hilliard L. Kutscher − *Advanced Cytometry Instrumentation System (ACIS), Amherst, New York 14260, United States; Division of Allergy, Immunology, and Rheumatology, Department of Medicine, Clinical Translational Research Center and Department of Anesthesiology, The State University of New York at Buffalo, Buffalo, New York 14203, United States*

Complete contact information is available at:
https://pubs.acs.org/10.1021/cbmi.3c00064

Author Contributions

All authors have given approval to the final version of the manuscript.

Notes

The authors declare no competing financial interest.

■ REFERENCES

(1) Pitts, N. B.; Zero, D. T.; Marsh, P. D.; Ekstrand, K.; Weintraub, J. A.; Ramos-Gomez, F.; Tagami, J.; Twetman, S.; Tsakos, G.; Ismail, A. Dental caries. *Nature Reviews Disease Primers* **2017**, *3* (1), 17030.

(2) Listl, S.; Galloway, J.; Mossey, P. A.; Marcenes, W. Global Economic Impact of Dental Diseases. *Journal of Dental Research* **2015**, *94* (10), 1355−1361.

(3) Cost-Effectiveness of Oral Diseases Interventions. https://www.cdc.gov/chronicdisease/programs-impact/pop/oral-disease.htm (accessed July 4, 2021).

(4) Mohanraj, M.; Prabhu, V.; Senthil, R. Diagnostic methods for early detection of dental caries - A review. *International Journal of Pedodontic Rehabilitation* **2016**, *1* (1), 29−36.

(5) Wenzel, A. Radiographic display of carious lesions and cavitation in approximal surfaces: Advantages and drawbacks of conventional and advanced modalities. *Acta Odontologica Scandinavica* **2014**, *72* (4), 251−264.

(6) Wenzel, A.; Larsen, M. J.; Feierskov, O. Detection of Occlusal Caries without Cavitation by Visual Inspection, Film Radiographs, Xeroradiographs, and Digitized Radiographs. *Caries Research* **1991**, *25* (5), 365−371.

(7) Bader, J. D.; Shugars, D. A. A systematic review of the performance of a laser fluorescence device for detecting caries. *Journal of the American Dental Association* **2004**, *135* (10), 1413−1426.

(8) Abiodun-Solanke, I.; Ajayi, D.; Arigbede, A. Nanotechnology and its application in dentistry. *Ann. Med. Health Sci. Res.* **2014**, *4* (9), 171−177.

(9) Chen, G.; Qiu, H.; Prasad, P. N.; Chen, X. Upconversion nanoparticles: design, nanochemistry, and applications in theranostics. *Chem. Rev.* **2014**, *114* (10), 5161−214.

(10) Jalani, G.; Tam, V.; Vetrone, F.; Cerruti, M. Seeing, Targeting and Delivering with Upconverting Nanoparticles. *J. Am. Chem. Soc.* **2018**, *140* (35), 10923−10931.

(11) Tanzer, J. M.; Livingston, J.; Thompson, A. M. The microbiology of primary dental caries in humans. *J. Dent Educ* **2001**, *65* (10), 1028−37.

(12) Bikker, F. J.; Cukkemane, N.; Nazmi, K.; Veerman, E. C. I. Identification of the hydroxyapatite-binding domain of salivary agglutinin. *European Journal of Oral Sciences* **2013**, *121* (1), 7−12.

(13) Fang, W.; Wei, Y. Upconversion nanoparticle as a theranostic agent for tumor imaging and therapy. *Journal of Innovative Optical Health Sciences* **2016**, *09* (04), 1630006.

(14) Li, Z.; Zhang, Y. An efficient and user-friendly method for the synthesis of hexagonal-phase NaYF 4:Yb, Er/Tm nanocrystals with controllable shape and upconversion fluorescence. *Nanotechnology* **2008**, *19* (34), 345606.

(15) Boyer, J.-C.; Vetrone, F.; Cuccia, L. A.; Capobianco, J. A. Synthesis of Colloidal Upconverting NaYF4 Nanocrystals Doped with Er3+, Yb3+ and Tm3+, Yb3+ via Thermal Decomposition of Lanthanide Trifluoroacetate Precursors. *J. Am. Chem. Soc.* **2006**, *128* (23), 7444−7445.

(16) Bogdan, N.; Vetrone, F.; Ozin, G. A.; Capobianco, J. A. Synthesis of Ligand-Free Colloidally Stable Water Dispersible Brightly Luminescent Lanthanide-Doped Upconverting Nanoparticles. *Nano Lett.* **2011**, *11* (2), 835−840.

(17) Wang, F.; Liu, X. Upconversion Multicolor Fine-Tuning: Visible to Near-Infrared Emission from Lanthanide-Doped NaYF4 Nanoparticles. *J. Am. Chem. Soc.* **2008**, *130* (17), 5642−5643.

(18) Karvianto, u.; Chow, G. M. The effects of surface and surface coatings on fluorescence properties of hollow NaYF4:Yb,Er upconversion nanoparticles. *J. Mater. Res.* **2011**, *26* (1), 70−81.

(19) Boyer, J.-C.; van Veggel, F. C. J. M. Absolute quantum yield measurements of colloidal NaYF4: Er3+, Yb3+ upconverting nanoparticles. *Nanoscale* **2010**, *2* (8), 1417−1419.

(20) Nadort, A.; Zhao, J.; Goldys, E. M. Lanthanide upconversion luminescence at the nanoscale: fundamentals and optical properties. *Nanoscale* **2016**, *8* (27), 13099−130.